An Automatic Measurement System for the Evaluation of Carotid Intima-Media Thickness

Consolatina Liguori, *Member, IEEE*, Alfredo Paolillo, and Antonio Pietrosanto, *Member, IEEE*

***Abstract*—This paper presents an automatic system for the measurement of carotid intima-media thickness (IMT) that is based on the digital processing of ultrasound images. The measurement technique is described in detail, highlighting the advantages compared to other methods and, reporting some experimental results. Finally, an analytical approach is used to estimate the intrinsic accuracy of the system.**

***Index Terms*—Boundary detection, carotid plaque, feature extraction, image processing, medical applications, thickness measurements, ultrasonic.**

I. Introduction

OVER THE last few years, image processing has been playing an increasingly important role in many scientific areas [1], [2]. This is due, among other reasons, to the ever-improving performance of computers that are now capable of quickly processing the characteristically large amounts of data produced by images. This processing is mostly oriented toward extracting either qualitative or quantitative morphological information from object images. In particular, precise dimensional characterization of objects through contact-less measurement techniques is a very important task in several environments such as industrial quality and process control [3] and medical diagnosis.

A typical application field of medical image processing is in the diagnosis of atherosclerosis [4]. The latter is a process of arterial degeneration, which starts, generally, in infancy, but is detected only in adulthood and whose consequences (cerebral infarction, embolus, ictus, ischaemia) are the main causes of death in the western world.

The atherosclerosis process is strongly linked to carotid thickening and plaques, whose presence can be clearly detected in artery longitudinal section images provided by ultrasound techniques. The analysis of the carotid ultrasound image represents, in fact, the most powerful instrument today available for predicting coronary disorders in people over fifty [5], [6].

Images are taken by ultrasound equipment working at frequencies ranging from 1 to 20 MHz, and are obtained via a probe that has to be positioned on the patient's neck. There are two phases to the measurement process: i) carotid image capturing and ii) thickness measurement.

i) The human operator suitably places the ultrasound probe in a position that gives a noiseless and clear image of the required part of the carotid. The choice of ultrasound frequency value is important since it ensures the best compromise between resolution and investigation space. The operator stops the acquisition and captures the image only when it satisfies measurement expectations. Image quality depends both on operator skill and patient tissue characteristics. The final result of this phase is characterized by very low repeatability due not only to this reason but also to the natural variability of arterial dimensions too.

ii) The operator then carries out thickness measurements using a track-ball to select measurement points on the leading edges of the captured ultrasound image. This phase too has low reproducibility and low accuracy mainly due to the poor ability of the human eye at detecting leading edges.

Since, at present, there is no automatic system able to carry out the human operations of phase i), carotid measurement improvements must be sought through developing suitable ultrasound image processing techniques. In particular, some techniques have already been developed for leading edge detection and for carotid intima media thickness (IMT) measurement. Some of them [7]–[9] work on tape-recorded images, and are still characterized by high operator interactivity and long running time. Cheng *et al.* [10] compared some algorithms for the detection of the layers of interest in carotid ultrasound images, but they limited their analysis to a graphical comparison rather than a quantitative metrological evaluation. Chan *et al.* [11] proposed a snake-like algorithm, with good results with respect to reference manual measurements, but the measurement uncertainties were not reported. Finally, in the paper of Liang *et al.* [12], where a quantitative evaluation of the proposed algorithm is performed, a discussion about calibration and its uncertainty is missing.

In this paper, a system for carotid IMT automatic measurements is proposed that fully automates phase ii). Moreover, it is also capable of working on images directly captured from the ultrasound equipment, thereby avoiding any image corruption eventually due to the tape recording. Thanks to the hardware adopted (a PC hosting a suitable frame grabber) and to the software developed, the measurement system is fast, precise and its interface is user-friendly. It also enables measurement results from images obtained on successive occasions from the same patient to be used for precise disease monitoring. In the next sections, the measurand and the medical problem are briefly discussed; the measurement technique and the software are de-

Manuscript received May 4, 2000; revised September 30, 2001.

C. Liguori is with DAEIMI, University of Cassino, Cassino, FR, Italy (e-mail: liguori@unicas.it).

A. Paolillo and A. Pietrosanto are with DIIIE, University of Salerno, Fisciano, SA, Italy (e-mail: apaolillo@unisa.it; apietrosanto@unisa.it).

Publisher Item Identifier S 0018-9456(01)10975-7.

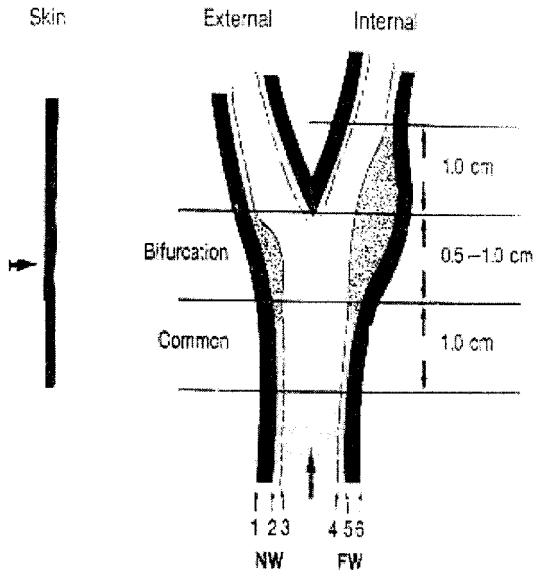

Fig. 1. Drawing of the carotid artery, with the interfaces: 1) periadventitia–adventitia (NW), 2) adventitia–media (NW), 3) intima–lumen (NW), 4) lumen–intima (FW), 5) media–adventitia (FW), 6) adventitia–periadventitia (FW).

scribed in detail, and some experimental results are given. Finally, the accuracy of carotid artery measurements is analyzed.

II. The Measurand

In Fig. 1, the carotid artery longitudinal section is drawn. Each carotid artery is characterized by a longitudinal tract (common carotid) that, after an enlargement (carotid sinus) containing a flow divider, bifurcates into two arteries, one internal and one external, on the basis of their position in relation to neck skin. Artery walls are made up of three layers (or *tunicae*): *intima*, *media*, and *adventitia*. The tunica intima is composed of a single layer of flattened epithelial cells with an underlying basement membrane. The tunica media comprises an inner layer of elastic fibers and an outer layer of circular smooth muscle. The tunica adventitia is composed of collagenous fibers. In ultrasound impulse-based analysis, blood (arterial lumen) and wall layers exhibit differences in wave reflection capability due to differences in density and elasticity.

Hence, the arterial lumen and tunica media do not reflect ultrasound waves, thereby allowing the intima–lumen and adventitia–media interfaces to be identified. The longitudinal scansion of the common carotid allows three interfaces to be highlighted for each of the two walls (near wall and far wall). Starting from the upper side of the image: the first line edge 1) corresponds to the external surface of the adventitia layer (also called periadventitia-adventitia layer), the second one 2) to the adventitia–media interfac, and the third one 3) is the intima–lumen interface. The fourth down is the far wall, coming from inside the artery instead of outside. This implies that the same interfaces of the near wall are found but in an inverse order: the first one 4) is the lumen–intima interface, the second 5) is the media–adventitia interface, and the third 6) is the external surface of the adventitia layer.

The main symptom of atherosclerosis (found in different ages and races of people) is the carotid intima layer thickening in proximity to the endotelial lumen surface. This thickening can be also confined to a short artery segment, and in this case, it is called plaque. It can be detected and evaluated by measuring intima–media thickness, which can be defined as the distance between 2) and 3) for the near wall, and between 4) and 5) for the far wall. Reference values of the intima–media thickness (IMT) are the following:

— Normal: $\text{IMT} < 1.0$ mm;
— Thickening: $1.0\text{ mm} < \text{IMT} < 1.3$ mm;
— Plaque: $\text{IMT} > 1.3$ mm.

Further considerations must be made about the orientation of the longitudinal section of the common carotid with respect to a coordinate system based on rows and columns of the ultrasonic image. To the human eye, it looks parallel to the horizontal axis. In practice, since the ultrasonic probe is always placed by the human operator on the external surface of the patients neck, the orientation depends only on the position of the artery with respect to the neck longitudinal axis. The common part of the carotid artery can be considered parallel to the neck axis in most people, thus allowing approximation of the above-mentioned thickness and diameters with distances on the vertical axis. However, in order to evaluate the maximum error introduced by this approximation, the angle between the common carotid longitudinal axis and the image horizontal axis was measured by the authors on 34 different patients. The mean value was equal to 3.3° with $\sigma = 2.2°$; this means that considering a typical 6 mm carotid diameter the mean error is equal to 0.01 mm, thus much lower than the required resolution (0.1 mm).

III. Automatic Measurement System

First, the human operator must obtain and capture a noiseless and clear image of the required part of the carotid on the ultrasound equipment display. Then, since the image scale factor depends on the probe ultrasound frequency and the frequency value can be changed at each acquisition, the human operator is also required to draw with the ultrasound equipment track-ball two 10.0 mm segments (a vertical and a horizontal) in a corner of the captured image. These two segments contained in the captured image will be used by the image processing software to calculate the pixel-millimeter conversion factor. All successive operations are entrusted to the image processing system.

The proposed measurement system hardware (see Fig. 2) is based on a computer (Intel Pentium™ 166 MHz) and on a suitable device for digital image grabbing that can be connected both directly to the ultrasound equipment and to a video-recorder. Since both ultrasound equipment and video-recorders usually have PAL/NTSC standard composite-video output ports, the computer hosts a frame grabber card (MRT Video Port Professional™ with 922×576 pixels maximum resolution), which converts the analog composite video signals into three image pixel matrices [$I_R(y, x)$, $I_G(y, x)$, $I_B(y, x)$], at each software trigger command. The

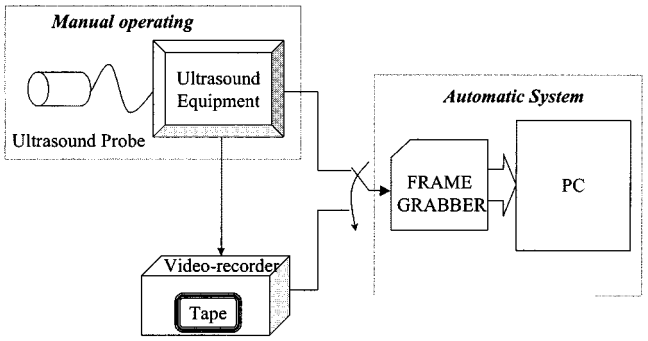

Fig. 2. Block scheme of the measurement station.

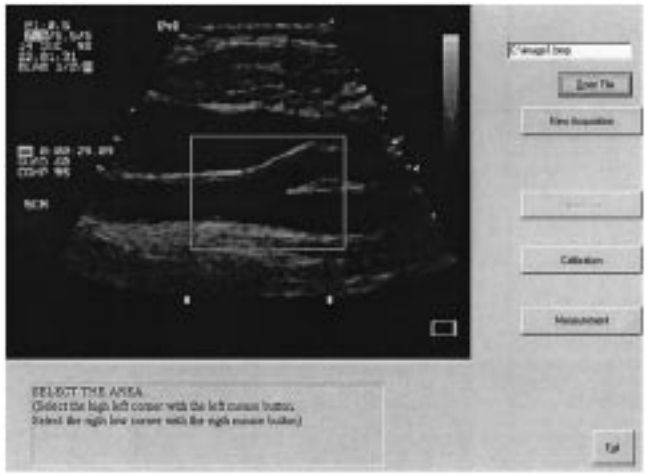

Fig. 3. Area selected by the operator in the captured image.

implemented software can be subdivided into two main parts: the user-interface and processing routines.

A. The User Interface

The user interface is made of some virtual panels allowing the user to interact with the measurement system in order to: select the image of interest, calibrate the probe, choose the measurements to be carried out, and collect results. A suitable virtual button allows the image capture to be triggered by the user while displaying the video signal in a front panel window (Fig. 3). The set of measurements on the carotid transversal section to be implemented was determined in agreement with medical scientists and technicians from the University of Naples and private clinics. The measurements of intima-media thickness for each wall (near and far), the lumen–lumen diameter and the adventitia–adventitia diameter were required, even though one wall (near or far) analysis can be considered sufficient in some cases. Moreover, these measurements usually concern only a short tract of the whole image, where the thickening could be supposed. On this basis, at first the software requires the user to draw a rectangle with the computer mouse to select the region of interest (ROI) for the image analysis, thus simplifying the task of the image segmentation software. Then, the detected adventitia–media and intima–lumen interfaces of both walls or just one, depending on the user choice, are underlined on the image. Finally, while a scroll-bar allows the user to select with one pixel resolution any cross-section of the carotid in the ROI, the corresponding values of the above-mentioned measurements for each position of the cursor are indicated in appropriate windows (Fig. 4).

B. Image Processing

The image processing-based measurement software is the basis of the functional features and performance of the measurement system. It implements original algorithms, which were designed specifically and set up by the authors for this application. The core of the measurement software is composed of the pattern recognition and edge detection (PRED) algorithm and the measurement algorithm.

The PRED algorithm has the task of finding, in the user-selected area, all the pixels belonging to the two required interfaces (lumen–intima and media–adventitia) for each wall.

It begins with the image format conversion: the 24-color RGB image $[I_R(y, x), I_G(y, x), I_B(y, x)]$ coming from the frame grabber card is converted to a monochromatic image $I(y, x)$ by the weighted mean relationship: $I(y, x) = 0.299 * I_R(y, x) + 0.587 * I_G(y, x) + 0.114 * I_B(y, x)$ [13]; then, a new intensity matrix $I_A(y, x)$ is extracted from $I(y, x)$, by considering only pixels internal to the ROI.

Then, the interface identification is provided by an algorithm suitably designed for the carotid ultrasound image processing. Since, in an ideal carotid artery, ultrasound image all the pixels corresponding to the lumen are anecoic and the tunica intima and tunica adventitia are the most reflective layers, the intensity gradient along a column of $I_A(y, x)$ versus the row index (y) would have the evolution of Fig. 5. It is possible to note that the lumen corresponds to rows where the gradient is constant and equal to zero. Starting from one of these pixels and moving toward the near wall, the lumen–intima interface corresponds to the first relative minimum and the media–adventitia interface to the second relative minimum. Vice versa, moving toward the far wall, the lumen–intima interface corresponds to the first relative maximum and the media–adventitia interface to the second one. In the practice, both lumen and layers are not so clear and noiseless, as is shown in Fig. 6, where the intensity gradient versus the row index for a column of the image of Fig. 3 is reported. As a matter of fact, lumen anecoic pixels are generally characterized by intensity levels close to 0 (black), but some blood turbulence may appear as gray spots in the lumen that generate edges in the gradient evolution, and consequently reduce the reliability of the gradient-based lumen–intima interface pixel detection.

Human technicians are skilled enough to recognize blood turbulence from thickening mainly on the basis of the gray level and of the shape. Layers (tunicae) generate high-intensity echoes (this means white pixels in the ultrasound image), and always assume a smoothed longitudinal profile, even in the presence of plaques. In order to reproduce this sensitivity, a statistical approach was adopted. A high number (133) of ultrasound carotid images, acquired by different equipment and technicians, have been examined through the analysis of the ROI gray level histogram, where a class width equal to 5 is used. This statistical treatment led to the following observations: i) the gray distribution is always mono-modal asymmetric; ii) pixels corresponding to blood or other nonreflective substances are contained in a few classes around the mode and amount to

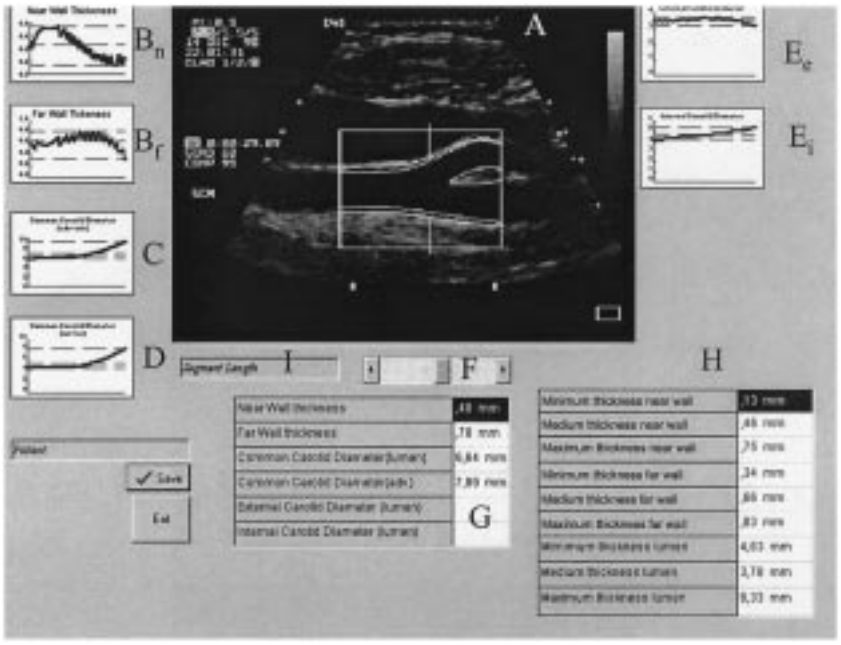

Fig. 4. Output panel. A) The interfaces found in the user selected area of the captured image; B) IMT trend for near (Bn) and far (Bf) wall; C) adventitia–adventitia common carotid diameter trend; D) intima–intima common carotid diameter trend; E) intima–intima external carotid diameter trend (Ee) and intima–intima internal carotid diameter trend (Ei); F) scrollbar for the **x** value at which the measurement values refer; G) measured value table; H) statistical representation of data concerning the analyzed area; I) cursor for user defined measurement.

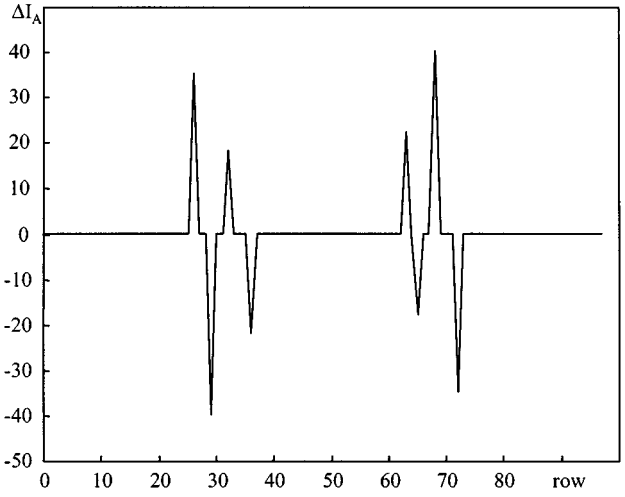

Fig. 5. Expected I_A vertical gradient.

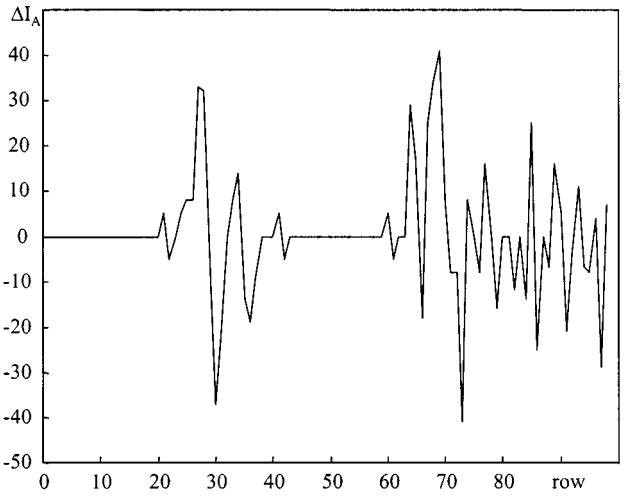

Fig. 6. Measured I_A vertical gradient.

at least 60% of the total image pixels; iii) pixels corresponding to tunicae and tissues are dispersed in all the other classes; iv) a relative minimum divides the two groups of classes. On the basis of these observations, it was decided to filter the image before the edge detection by zeroing all the pixels whose intensity is lower than the threshold th

$$\textbf{if} \quad I_A(y, x) < th \qquad \textbf{then} \quad I_A(y, x) = 0.$$

Here, for each image, th is equal to the intensity level corresponding to the lower extremity of the first nonempty class that comes in the histogram after the cumulated frequency has reached 60%. See Fig. 7 where the relative and cumulated frequencies of the intensity level histogram concerning the ROI of Fig. 3 are reported. Most of the blood turbulences are filtered by this image pre-processing. Residuals isolate white pixels that should be kept close. Black holes generated along the lumen–intima edge are removed by the edge detector on the basis of their distances from the neighborhood edge pixels. In practice, the row index $y(i)$ of each pixel $P_i \equiv (y(i), x(i))$ first selected by the aforementioned criteria (see Fig. 8 stars) is compared with the value $y_m(i)$, obtained by averaging the last four edge pixel row indices [$y_m(i) = (1/4)\sum_{k=-3}^{0} y(i+k)$]. If their difference is greater than 2, the pixel row index of the lumen–intima edge pixel is substituted with the averaged one

$$\textbf{if} \quad |y(i) - y_m(i)| > 2 \qquad \textbf{then} \quad y(i) = y_m(i)$$

thus giving as a result a smoothed noiseless edge (Fig. 8 line). This length (4) proved to give the best compromise between ro-

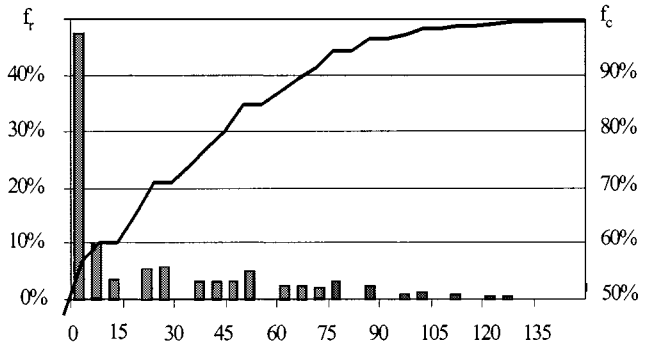

Fig. 7. Relative f_r and the cumulate frequency f_c of I_A gray level.

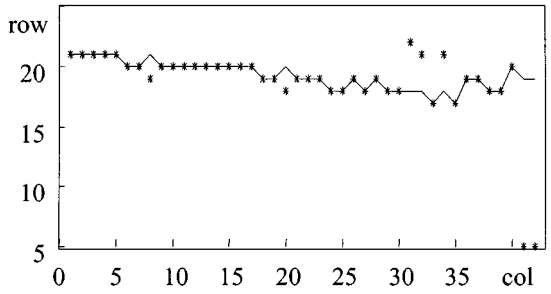

Fig. 8. The lumen–intima edge points without (∗) and with (−) the filtering.

bustness and computational burden, in the whole set of experiments.

As for the media–adventitia interface, the intensity gradient versus row index (see Fig. 6) can also lead to the edge detection. For each column, the media–adventitia edge pixels come to be identified respectively as the vertical gradient absolute minimum for the near wall, and the vertical gradient absolute maximum for the far wall. The above-mentioned smoothing operator also contributes in this case to obtain a noiseless edge detection.

The measurement algorithm determines the diameter of lumen and tunica–media, and the intima–media thickness of the near and far wall. For each column of the selected area, distances between the corresponding edge points are defined as the number of pixels and so as the difference between row indices. As a result, the diameters and thickness are evaluated as the product between a number of pixels and the constant conversion factor obtained in the calibration. This simplified algorithm gives good results in the case of common carotid artery measurements (as mentioned in Section II). Whenever either external or internal carotid artery measurements should be required, since these two arteries are significantly misaligned with respect to the patient's neck, the selection on the virtual panel of the external/internal carotid measurement executes the following measurement algorithm.

i) The LSM first-order regression of the far wall media–adventitia edge pixels is calculated.
ii) The equation of the family of orthogonal lines is calculated.
iii) The thickness and diameter are then defined by the simple application of the Pitagora formula to couples of edge points given by the intersection of corresponding layers with one of the orthogonal lines. This means that $s = \sqrt{k_x^2 N_x^2 + k_y^2 N_y^2}$, where: k_x and k_y are the horizontal and vertical calibration constants, N_x is the difference of the pixel column indices and N_y is the difference of the pixel row indices of the two edge points.

TABLE I
MAXIMUM STANDARD DEVIATION OF INTIMA–MEDIA THICKNESS MEASUREMENTS FOR DIFFERENT INTERFACE TYPES

Interface type	σ [mm]
Linear	0.05
Curve	0.05
Plaques	0.09

TABLE II
NEAR AND FAR WALL INTIMA–MEDIA THICKNESS MEASUREMENTS CARRIED OUT BY: THE PROPOSED AUTOMATIC MEASUREMENT SYSTEM (AMS), AND BY THE PROSOUND

Near wall		Far wall	
Prosound mm	AMS mm	Prosound Mm	AMS mm
0.825	0.82	0.701	0.68
1.192	1.19	1.108	1.12
0.704	0.69	0.741	0.72
0.847	0.83	0.755	0.74
0.766	0.75	0.834	0.84
1.007	1.03	1.113	1.13
0.967	0.99	0.700	0.68
0.801	0.82	0.696	0.68
0.973	0.95	1.165	1.15
0.860	0.85	1.111	1.12
0.819	0.79	0.850	0.84
1.172	1.19	1.265	1.28
0.695	0.68	0.810	0.79
1.051	1.06	0.664	0.68
0.939	0.95	0.789	0.77
1.277	1.28	1.071	1.09
0.821	0.84	0.865	0.88
0.840	0.84	1.038	1.05
1.017	1.02	1.026	1.04
1.312	1.32	1.091	1.11

IV. SOME METROLOGICAL CONSIDERATIONS

As evidenced in the Introduction, the patient carotid image capture [phase i)] is characterized by high variability which depends on the natural cardiac organ activity and on the human interactions with the ultrasound probe and equipment. The quantitative evaluation of this variability could be very cumbersome and give results depending on the way the tests are carried out.

Phase ii) of the measurement process is instead based on repeatable and controllable phenomena, thus allowing a significant evaluation of measurement uncertainty. In the following, an analytical evaluation of the standard uncertainty is made. This *a-priori* analysis [14], [15] consists of the application of the ISO-GUM uncertainty propagation law [16] to the measurement algorithm.

For the sake of brevity, only the case of common carotid measurement is reported. As a consequence, we are interested in the

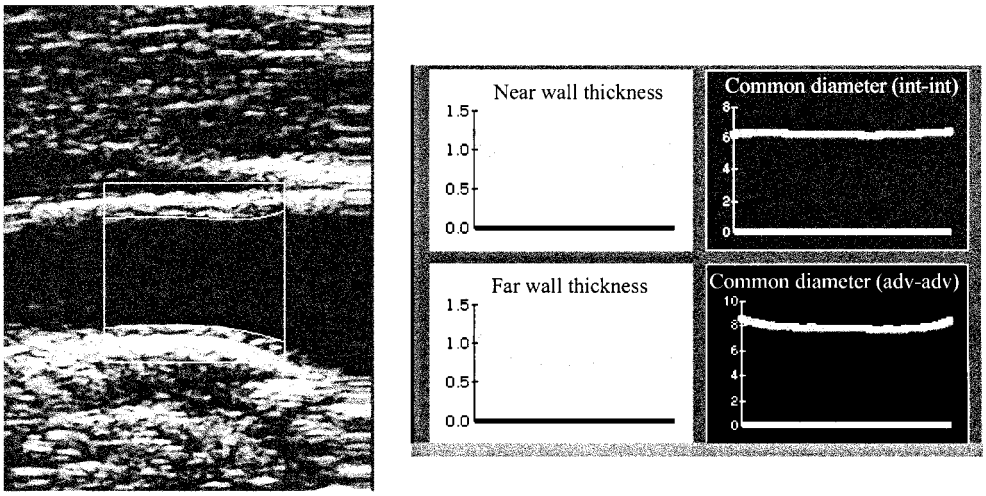

Fig. 9. Near and far wall analysis of a common carotid artery.

uncertainty of thickness and diameter measurements, which are both expressed by relationships like this

$$s = k \cdot N_y \tag{1}$$

where k is the constant conversion factor, and N_y is the measured length of the identified vertical segment, expressed in the number of pixels.

Supposing these two terms are not correlated, and applying the ISO-GUM uncertainty propagation law to (1), we have that the uncertainty of the measurement of s (U_s) is given by the following relationship

$$U_s = \sqrt{k^2 \cdot U_{Ny}^2 + N_y^2 \cdot U_k^2} \tag{2}$$

and so depends on U_k and U_{Ny}.

As for U_{Ny}, we can show (see Appendix) that

$$U_{Ny} = \frac{1}{2 \cdot \sqrt{6}}. \tag{3}$$

As far as U_k is concerned, given that ℓ_m [m] and N_ℓ [N of pixels] are both measurements of the calibration segment length, respectively made by the ultrasound equipment and the measurement software, we have

$$k = \frac{\ell_m}{N_\ell} = \frac{\text{m}}{\text{pixel}} \tag{4}$$

and

$$U_k^2 = \frac{\ell_m^2}{N_\ell^4} U_{N_p}^2 + \frac{1}{N_\ell^2} U_{\ell_m}^2. \tag{5}$$

For U_{N_ℓ} we have (see Appendix):

$$U_{N_\ell} = \frac{1}{2 \cdot \sqrt{12}}. \tag{6}$$

While the uncertainty of ℓ_m depends on the accuracy (A) of the ultrasound equipment, considering the uniform probability distribution we have:

$$U_{\ell_m} = \frac{A}{\sqrt{3}}. \tag{7}$$

To quantify these relationships, given a calibration segment $\ell_m = 10$ mm, corresponding to $N_\ell = 100$, it would be $k = 100.0 \cdot 10^{-6}$ m/pixel. If $A = 0.05$ mm, then $U_k \cong 0.2 \cdot 10^{-6}$ m/pixel. And consequently for a distance $s = 1.00$ mm, corresponding to $N_y = 10$, we would have $U_s \cong 0.02$ mm.

V. Experimental Results

Several tests were made on images acquired using different ultrasound systems and by different human operators in order to verify the robustness and the reliability of the image processing software. Images were captured using the following equipment: i) ATL HDI 5000 equipped with a 5–7.5 MHz probe; ii) an HP SONOS Phased Array equipped with a 5–12 MHz probe; iii) BIOSOUND (Esaote, Inc.) with a 5–12 MHz probe.

First, the robustness of the edge detection algorithm has been evaluated in terms of sensitivity to the ROI: given an image, 20 intima–media thickness measurements are carried out on the same point of the arterial by selecting different ROI. The standard deviation of measurements quantifies the sensitivity to the ROI. This operation has been performed on about 30 images, in order to explore the influence of the type of intima–lumen interface (linear, curve or plaque). Results are given in Table I where the maximum value of the intima–media thickness standard deviation is reported for each interface type.

Then, the correlation between manual and automated intima–media thickness measurements was evaluated by calculating the following quantity $c(\mathbf{x}, \mathbf{y})$ as shown in the equation at the bottom of the next page, where $\mathbf{x}$ is a set of $N = 20$ intima–media thickness measurements made by a skilled technician, and $\mathbf{y}$ is the corresponding set of measurements made by the proposed software. The result of 0.97 shows a very good agreement between the two sets, and it is better than values obtained by several other methods [17].

Finally, a direct comparison was made with another measurement software, PROSOUND, developed at the University of Southern California by Robert Salzar for the NASA Technology Transfer Program. A sample of 20 intima–media thickness measurements performed by both software programs on the same

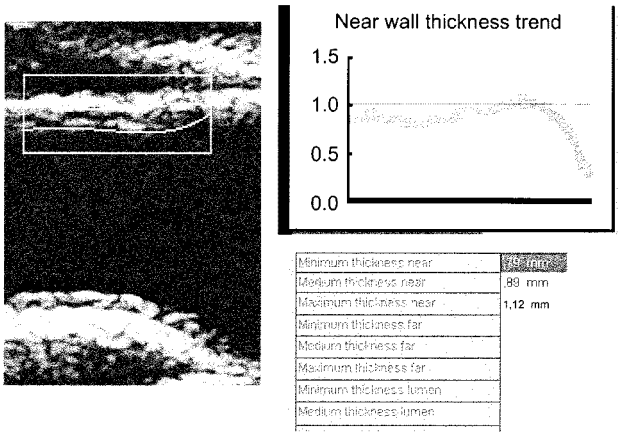

Fig. 10. Near wall analysis showing a low intima–media thickening.

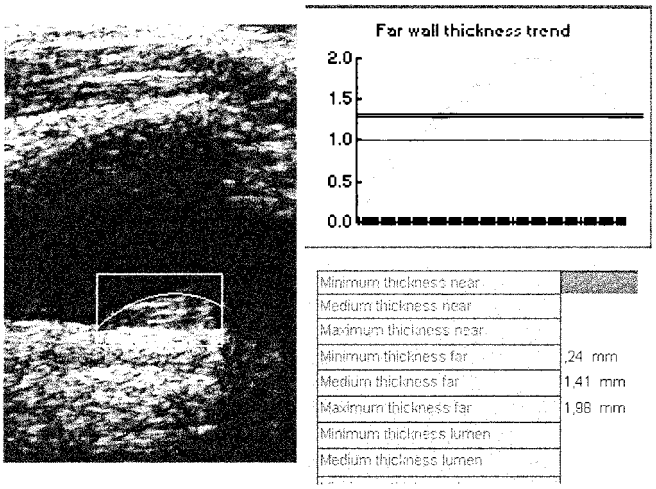

Fig. 11. Far wall analysis showing a significant plaque.

images is reported in Table II. The measurements proved to always be compatible, thus excluding systematic errors higher than the measurement uncertainty (0.2 mm).

Finally, a sample of the total number of experimental results obtained is presented in the following. Fig. 9 shows a zoom view of the results for a near and far wall analysis of a common carotid artery characterized by regular thickness of both walls. In Fig. 10, the near wall thickness trend diagram allows the thickening of the near wall to be detected; because of its low magnitude, the phenomenon would hardly have been recognized by the human eye analysis. Furthermore, in Fig. 11 an evident plaque is detected on the far wall, and its thickness is measured with 0.01 mm resolution. It should be noted that blood turbulence too close to the lumen–intima interface can sometimes look like plaque. In these cases, the nature of the thickening can be deduced only by analyzing successive images of the same carotid tract. As a consequence, the edge detector was tuned to its maximum sensitivity in order to detect and measure all the visible thickenings, leaving only the task of their recognition to the human operator.

VI. Conclusion

A PC-based image processing system for the measurement of carotid intima–media thickness has been presented, that works on arterial images provided by ultrasound equipment. The system is a substitute for the human technician in the detection of layers in the longitudinal section image, and the ultrasound equipment in the measurement of traced thickenings. Intima–media thickness and arterial diameter are measured with 0.02 mm standard uncertainty and without significant bias, as evidenced by results of comparisons with manual and automated measurements, thus allowing the immediate diagnosis of thickenings. The automation of the detection and measurement process grants high repeatability and accuracy in intima–media thickness measurements independently of the human technician expertise. Other similar systems, even though showing the same metrological performance, either require more interactions with the human technician or do not allow working with multiple frequency ultrasound equipment. Further efforts will be directed to implementing a patient disease-monitoring feature based on periodic intima–media thickness measurements.

Appendix

The uncertainty of N_y (U_{Ny}) can be evaluated by considering that if distance measurements are made between edge pixels with the same column index, then we have

$$N_y = y_2 - y_1 \tag{A1}$$

where y_1 and y_2 are the row indices of the two pixels. The indices can be considered statistically independent because they are obtained separately from two edge detection procedures.

As a result

$$U_{Ny} = \sqrt{U_{y1}^2 + U_{y2}^2}. \tag{A2}$$

In this framework, a simplification will be made about each U_{y_i}: even though it depends on the image noise, on the edge detection algorithm and other influence parameters [18]–[20], only

$$c(\mathbf{x}, \mathbf{y}) = \frac{N\sum_i x_i \cdot y_i - \sum_i x_i \cdot \sum_i y_i}{\sqrt{N\left(N\sum_i x_i^2 - \left(\sum_i x_i\right)^2\right) \cdot \left(N\sum_i y_i^2 - \left(\sum_i y_i\right)^2\right)}}$$

the spatial quantization process will be taken into account. According to other quantization processes (see A/D converters), the quantization error of each y_i ranges between $-1/2$ pixel and $+1/2$ pixel with confidence level 1 and triangular probability distribution [21]. As a consequence, since the standard uncertainty is equal to the standard deviation of the probability distribution

$$U_{yi} = \frac{1}{2 \cdot \sqrt{12}}. \tag{A3}$$

Consequently by substituting (A3) in (A2)

$$U_{Ny} = \frac{1}{2 \cdot \sqrt{6}}. \tag{A4}$$

For U_{N_ℓ}, the same considerations of U_{Ny} are still applicable, but the correlation between the segment extremities can not be considered null since the human operator is guided by the length measurement given by the ultrasound equipment in drawing the 10 mm segment. The correlation factor was empirically deduced from the direct evaluation of the uncertainty U_{N_ℓ}. On about 70 drawings of the calibration segment made by the same human operator, the following measurement uncertainty resulted:

$$U_{N_\ell} = \frac{1}{2 \cdot \sqrt{12}}. \tag{A5}$$

This means that a $-1/2$ correlation factor should be considered in the uncertainty propagation formula.

ACKNOWLEDGMENT

The authors wish to thank Dr. P. Guarini, "Villa dei Fiori" Hospital, Naples, Italy, and Dr. M. De Michele, of the Department of Clinical and Experimental Medicine at Naples "Federico II" University for their cooperation in helping to understand the medical problem. The authors would also like to thank G. Betta for his useful suggestions and to D. Capriglione for help with the experimental work.

REFERENCES

[1] R. Chelappa *et al.*, "The past, present, and future of image and multidimensional signal processing," *IEEE Signal Processing Mag.*, vol. 15, pp. 21–58, Mar. 1998.

[2] D. H. Ballard and C. M. Brown, *Computer Vision*. Englewood Cliffs, NJ: Prentice-Hall, 1982.

[3] L. Angrisani, P. Daponte, C. Liguori, and A. Pietrosanto, "An image based measurement system for the characterization of automotive gaskets," *Measurement*, vol. 25, pp. 169–181, 1999.

[4] M. G. Bond and S. K. Wilmoth *et al.*, "Detection and Monitoring of Asymptomatic Atherosclerosisi in Clinical Trials," *Amer. J. Med.*, vol. 86, (suppl 4A), pp. 33–36, 1989.

[5] N. M. El-Barghouty, T. Levine, S. Ladva, A. Flanagan, and A. Nicoladeis, "Histological verification of computerized carotid plaque characterization," *Eur. J. Vascular Endovascular Surg.*, vol. 11, pp. 414–416, 1996.

[6] T. Noritomi *et al.*, "Carotid plaque typing by multiple-parameter ultrasonic tissue characterization," *Ultrasound Med. Biol.*, vol. 23, pp. 643–650, 1997.

[7] N. M. El-Barghouty, T. Levine, S. Ladva, A. Flanagan, and A. Nicoladeis, "Histological verification of computerized carotid plaque characterization," *Eur. J. Vascular Endovascular Surg.*, vol. 11, pp. 414–416, 1996.

[8] T. Elatrozy, A. Nicoladeis, T. Tegos, and M. Griffin, "The objective characterization of ultrasonic carotid plaque features," *Eur. J. Vascular Endovascular Surg.*, vol. 16, pp. 223–230, 1998.

[9] P. J. Touboboul and P. Prati *et al.*, "Use of monitoring software to improve the measurement of carotid wall thickness by B-mode imaging," *J. Hypertension*, vol. 10, (suppl. 5), pp. S37–S41, 1992.

[10] D. Cheng, A. Schmidt-Truckäss, K. Cheng, M. Sandrock, Q. Pu, and H. Burkhardt, "Automatic detection of the intimal and the adventitial layers of the common carotid artery wall in ultrasound B-mode images using snakes," in *Proc. Int. Conf. Image Analysis Processing*, 1999, pp. 452–457.

[11] R. C. Chan, J. Khaufhold, L. C. Hemphill, R. S. Lees, and W. C. Karl, "Anisotropic edge-preserving smoothing in carotid B-mode ultrasound for improved segmentation and intima-media thickness (IMT) measurement," *Comput. Cardiol.*, vol. 27, pp. 37–40, 2000.

[12] Q. Liang, I. Wendelhag, J. Wikstrand, and T. Gustavsson, "A multiscale dynamic programming procedure for boundary detection in ultrasonic artery images," *IEEE Trans. Med. Imag.*, vol. 19, pp. 127–142, 2000.

[13] J. C. Russ, *The Image Processing Handbook*, 3rd ed. Piscataway, NJ: IEEE Press, 1999.

[14] G. Betta, C. Liguori, and A. Pietrosanto, "A structured approach to estimate the measurement uncertainty in digital signal processing algorithms," *Proc. Inst. Elect. Eng., Sci. Meas. Technol.*, vol. 146, pp. 21–26, 1999.

[15] M. De Santo, C. Liguori, and A. Pietrosanto, "Uncertainty characterization in image based measurements: A preliminary discussion," in *Proc. IEEE IMTC/99*, May 1999, pp. 947–952.

[16] "Guide to the expression of uncertainty in measurement (GUM)," Int. Stand. Org. (ISO), 1993.

[17] T. Gustavsson, R. Abu-Gharbieh, G. Hamarneh, and Q. Liang, "Implementation and comparison of four different boundary detection algorithms for quantitative ultrasonic measurements of the human carotid artery," *Comput. Cardiol.*, vol. 24, pp. 69–72, 1997.

[18] D. I. Havelock, "Geometric precision in noise-free digital images," *IEEE Trans. Pattern Anal. Mach. Intell.*, vol. PAMI-11, pp. 1065–1075, Oct. 1989.

[19] C. Ho, "Precision of digital vision systems," *IEEE Trans. Pattern Anal. Mach. Intell.*, vol. PAMI-5, Nov. 1983.

[20] S. Yi, R. M. Haralick, and L. G. Shapiro, "Error propagation in machine vision," *Mach. Vis. Applicat.*, pp. 93–114, 1994.

[21] B. Liu, "Effect of finite wordlength on the accuracy of digital filter—A review," *IEEE Trans. Circuit Theory*, vol. CT-18, 6, pp. 670–677, July.

Consolatina Liguori (M'98) was born in Solofra (AV), Italy, in 1969. She received the M.S. degree in electronic engineering from the University of Salerno, Salerno, Italy, in 1993. In 1997, she received the Ph.D. degree in industrial engineering at the University of Cassino, Cassino, Italy.

From 1997 to 2001, she was an Assistant Professor of electrical measurements at the University of Cassino. Since October 2001, she has been an Associate Professor of electrical measurements at the same university. Her interests are in the fields of digital signal and image processing, measurement system characterization, and artificial intelligence applications to measurements.

Alfredo Paolillo was born in Belvedere, Italy, in 1972. He received the degree in electronics engineering from the University of Salerno,Salerno, Italy, in 2000. He is currently pursuing the Ph.D. degree in information engineering in the Information and Electrical Engineering Department (DIIIE), University of Salerno.

His research activities include optical fiber temperature sensors and image-based measurement systems.

Antonio Pietrosanto (M'98) was born in Napoli, Italy, in 1961. He received the M.S. and Ph.D. degrees in electrical engineering from the University of Napoli, Napoli, Italy, 1986 and 1990, respectively.

In 1991 he became Assistant Professor and in 1999 Associate Professor of electrical and electronic measurements at the University of Salerno, Salerno, Italy. Since November 2001, he has been Full Professor of electrical and electronic measurements at the same university. His scientific interests are principally concerned with: instrument fault detection isolation and accommodation, digital signal and image processing for real-time diagnostic and process control, and fiber optic sensors.